Dynamic hyperconjugation induced bond-angle rotation isomerization mechanism and anionic conformational rigidity-dependent melting points of ionic liquids

*Lin Yuan[1], Aikifa Raza[1], Dimitrios Kyritsis[1], Hongbo Zeng[2], TieJun Zhang[1,]**

[1] Department of Mechanical Engineering, Masdar Institute,
Khalifa University of Science and Technology, P.O. Box 127788, Abu Dhabi, UAE

[2] Department of Chemical and Materials Engineering,
University of Alberta, Edmonton, AB, T6G 1H9, Canada

*correspondence authors: tiejun.zhang@ku.ac.ae

KEYWORDS: *Ionic Liquids, Phase Transition, Dynamic Effect, Conformational Rigidity, Stereochemistry.*

Abstract

The pyramidal inversion of trisubstituted heteroatoms is well-recognized. However, the stereochemistry of bicoordinated heteroatoms is poorly developed and few examples assumedly isomerize by double-torsion motion or bond-angle inversion. Here, by using *ab initio* molecular dynamics combined with metadynamics simulation, we reveal an unexpected competing isomerization mechanism, namely dynamic $\pi \rightarrow \sigma^*$ negative hyperconjugation induced coupled rotation of bond and bond angle leads to helix inversion in bis(trifluoromethane)sulfonamide ($TFSI^-$), making $TFSI^-$ follow four distinct *trans-cis*

isomerization pathways with diverse energy barriers (12–52 kJ mol^{-1}) which are significantly higher than 3.6 kJ mol^{-1} of sole pathway estimated by conventional static calculations. Our quantitative simulations and experiments results confirm the positive correlation between overall stability of *cis*-$TFSI^-$ with polarity of countercations. The melting points (T_m) of $TFSI^-$-based ionic liquids (ILs) linearly rise with the conformational rigidity of $TFSI^-$ in the ion pair state, offering a new fundamental perspective on the origin of low T_m of ILs.

Introduction

The pyramidal inversion **1**, a fundamental stereochemical process, is intensively studied and well-established in tricoordinated heteroatom compounds (X = N, O^+, P, S^+), which involves a planar transition state and thus sp^3-sp^2-sp^3 re-hybridization at the heteroatoms X (Scheme 1a)[1-4]. Many isolable phosphines[1] and sulfonium salts[4] possess high inversion energy barriers of 120–185 kJ mol^{-1} and 100–130 kJ mol^{-1}, whereas nitrogen pyramidal inversion is rapid and only takes 20–25 kJ mol^{-1} in a tertiary amine due to quantum tunnelling[5]. By contrast, the bond-angle inversion (BAI) **2** at a singly bonded atom[6], is much less exploited, though we have extended this isomerization mechanism to the bicoordinated heteroatoms in doubly bonded or conjugated systems. Nitrogen BAI (85–125 kJ mol^{-1})[7, 8] and rotation around C=N bond (210–250 kJ mol^{-1} barrier for photoinduced rotation[9, 10]) provide alternative concerted mechanism for (E/Z) stereoisomerization in imine $C(R_1R_2)=N(R_3)$ **3**. When nitrogen is merely conjugated with one of ligands, the BAI barrier drops to 55 kJ mol^{-1} in thionylimide HNSO **4**[11]. When nitrogen is conjugated with both ligands, the S-N-S inversion requires exceptionally low energy (5 & 30 kJ mol^{-1}) in

heterocumulene radical OSNSO **5**[8]**,** which is even lower than 40 kJ mol^{-1} for two torsional motions. B-O-B inversion **6** overcomes an unusually high barrier of 104 kJ mol^{-1}, which is still lower than that of the double-torsion pathway involving only 90° motions, in singly bonded (BF)O(BF)-quinoxalinoporphyrin, owing to the geometrical restraints from B-O-B encapsulation[6]. Although all these examples involve a linear transition state, the oxygen BAI and nitrogen BAIs are distinct in the numbers of valence electron, bonding characters with ligands, and thus re-hybridization processes of central atoms (sp^3-sp-sp^3 (O) vs. sp^2-sp-sp^2 (N)). To date, there are no progresses in identifying the isomerization mechanism for bicoordinated O or its valence isoelectronic atoms (e.g., S in disulfide[12, 13]) or ions (e.g., N^-) in the systems with conjugated M_1-X-M_2.

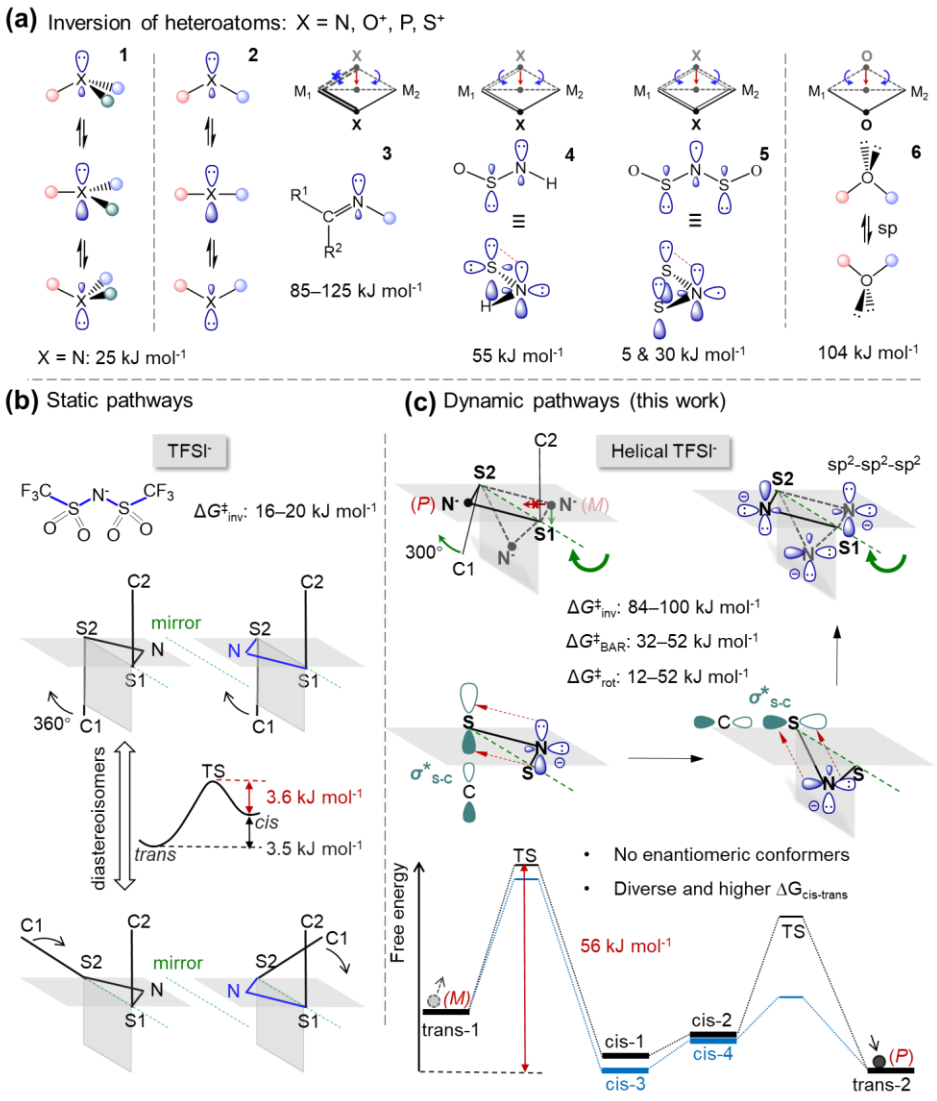

Scheme 1. Stereochemistry of heteroatoms. (a) Pyramidal inversion of tricoordinated heteroatoms **1**. Bond-angle inversion (BAI) (red arrows) of bicoordinated heteroatoms **2**, doubly bonded imine **3**, conjugated thionylimide HNSO **4** and heterocumulene radical OSNSO **5,** and singly bonded (BF)O(BF)-quinoxalinoporphyrin **6**. $\Delta G^{\ddagger}_{inv}$ for energy barrier of inversion, kJ mol^{-1}. Blue arrows for two torsional motions. (b) BAI and diastereomeric interconversion of TFSI^{-} anion with S–N^{-}–S moiety. (c) Dynamic π → σ*

negative hyperconjugation induced out-of-plane bond-angle rotation (BAR) leads to the helix inversion of $TFSI^-$ conformers. $\Delta G^{\ddagger}_{rot}$ for lone S–C bond rotation.

Centered with N^-, the anion bis(trifluoromethyl-sulfonyl)imide ($TFSI^-$) is assumed to be conjugated among $–SO_2–N^-–SO_2–$. N^- BAI only required 16–20 kJ mol^{-1} (Scheme 1b), estimated from the reported potential energy surface (PES)[14-17]. The two pairs of enantiomers of $TFSI^-$ (*trans* or *cis* isomers) with the only energy difference ($\Delta E_{cis\text{-}trans}$) of 3.5 kJ mol^{-1}, underwent diastereomeric interconversion over the sole torsional barrier ($\Delta E^{\ddagger}_{cis\text{-}trans}$) of 3.6 kJ mol^{-1}. [14-18] However, the barrier for rotation around single bond is about 12 kJ mol^{-1} in ethane[19], but 40 kJ mol^{-1} in radical OSNSO[8] and 85 kJ mol^{-1} in an amide[19] because of the conjugation effect. Moreover, previous theoretical studies on $TFSI^-$ and even all the BAI examples are limited to the static electronic structure calculation, a nonergodic, chemical-intuition-dependent approach, which is insufficient to rationalize or predict the isomerization/reaction mechanism involving unforeseen processes (e.g., coupled motions) while ignoring dynamic effects.[20-22] $TFSI^-$-based ionic liquids (ILs) exhibit multiple exotic thermal and mechanical properties, such as low melting points (a fingerprint of ILs)[23], peculiar sequence of phase transitions over temperature[24, 25], and pressure-induced liquid-liquid transition[26]. The conformational flexibility of $TFSI^-$ was considered to be one of possible driving factors. Nevertheless, the flexibility is inferred from the conventional theory for isolated $TFSI^-$ and not includes the impact of co-existing countercations in ILs.

Herein, we combine *ab initio* molecular dynamics (AIMD) simulation with metadynamics[27, 28] to explore the isomerization mechanism of isolated $TFSI^-$. Our simulations reveal that the conventional static conformation scanning approach significantly underestimated the restriction and complexity of $TFSI^-$ isomerization. $TFSI^-$ exhibits dynamic conformational rigidity with diverse energy barriers (12–52 kJ mol^{-1}) over four distinct *trans-cis* isomerization pathways. An unexpected isomerization mechanism, namely dynamic $\pi \rightarrow \sigma^*$ negative hyperconjugation enabled coupled rotation of bond and bond angle has been discovered for the first time, competing with other two fundamental intermolecular motions including bond rotation and bond-angle inversion (Scheme 1c). The concerted process provides a low-energy pathway for $TFSI^-$ to invert its helicity and form six diastereomeric conformers, rather than three pairs of enantiomers. We uncover that the overall stability of cis-$TFSI^-$ linearly increases with the polarity of countercations in the isolated ion pair state, by using metadynamics, an approach enhancing sampling while maintaining dynamic coupling with environments. The fractional population of *cis*-$TFSI^-$ follows the same trend in bulk ILs, which is confirmed by both experiments and simulations. In particular, we find that melting points of $TFSI^-$-based ILs is linearly dependent on the conformational rigidity of $TFSI^-$ in the ion pair state, rather than *cis*: *trans* ratio reported in molecular systems, or configurational entropy in BF_4^--based ILs. This indicates that the conformational rigidity can be used as a fundamental dynamic descriptor to quantify the disorder potential of ILs and provide a new perspective on the origin of low T_m of ILs and a guideline for the rational design of low-T_m ILs. The counterintuitive isomerization behavior of $TFSI^-$ and its correlation with distinct environments can also offer molecular level basis for multiple other unusual

thermal/mechanical/electrical properities of ILs, ranging from phase transition[24], phase-dependent interfacial capacitance[29], direct piezoelectric effect[30] to long-lived electric fields[31].

Results and Discussion

Conformational space of isolated $TFSI^-$. Figure 1a shows the torsional free-energy landscape over two torsion/dihedral angles for presenting the conformational space of isolated $TFSI^-$. The free-energy surface features that (1) the minima (stable/metastable states) and saddle points (transition states) are not symmetric with respect to the 180-180 diganol; (2) the saddle points are unexpectedly higher than the global minima, namely, $TFSI^-$ undergoes restricted isomerization with diverse and high energy barriers (12–52 kJ mol^{-1}). To explore the relationship between free energy and conformational structure, we take the structural snapshots corresponding to the characteristic points from metadynamics simulation. The conformations are displayed in the Newman projection, looking along the imaginary S-S axle (Figure 1 b). We have identified two independent pathways (**I & II**) for the *trans*-*trans* process and four *cis*-*trans* isomerization subpathways (**1–4**). In pathway **I**, starting with *trans*-B1, the coupled clockwise motion comprising S2–C1 bond rotation and 180° S–N–S bond-angle rotation (BAR) around the S-S axle, leads to the formation of *cis*-C1 **1**. Subsequently, S2–C1 bond continuously rotates to *trans*-D, whereas S–N–S bond angle just oscillates slightly relative to the horizontal plane. In pathway **II**, these two steps are reversed. Interestingly, the BAR occurring in each pathway induces the M(left-handed)-to-P(right-handed) helix inversion between *trans*-B1 (16 kJ mol^{-1}) and energetically more favorable *trans*-D (0 kJ mol^{-1}), accompanied by a unidirectional 300°

rotation of C1–S2 bond around the S-S axle. The unprecedented rotation/ocillation of S-N-S bond angle (Figure 1c), and the different sequences of these two motions in each pathway seem to enable all the conformers to be diastereomeric with each other, but why do the motions occur in $TFSI^-$ and are the *cis-trans* free-energy barriers unexpectedly higher and diverse?

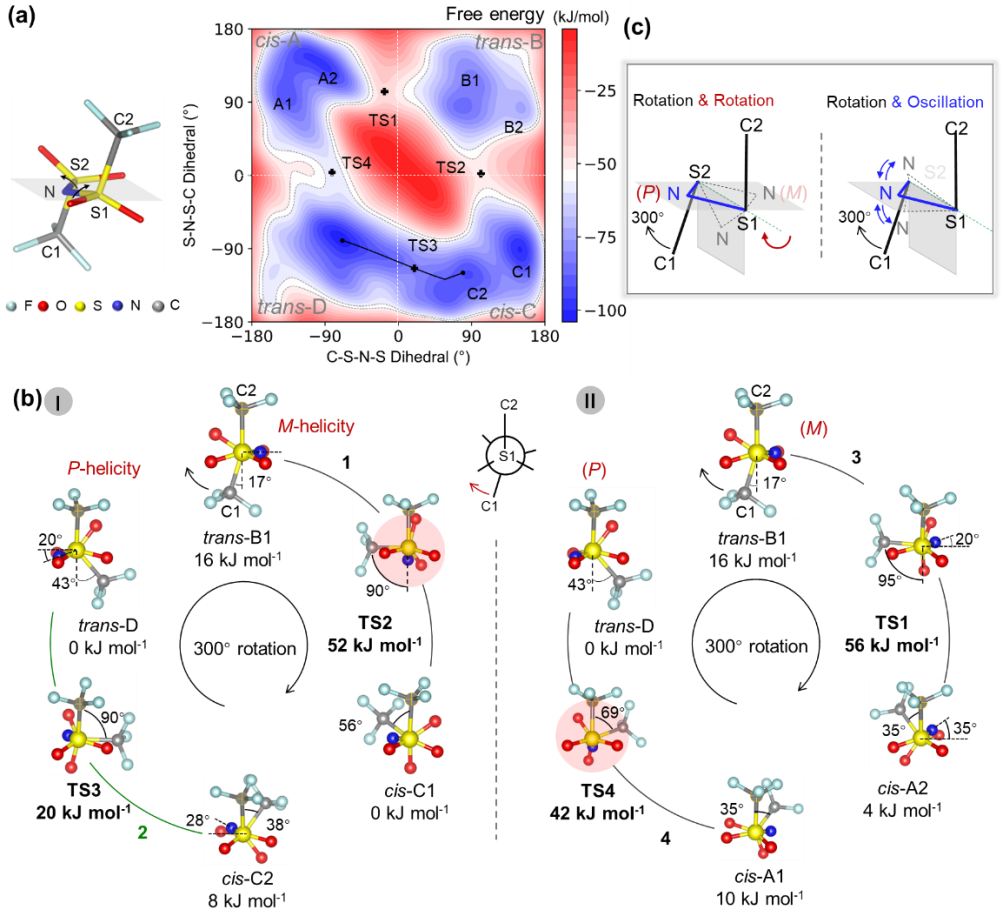

Figure 1. (a) Torsional free-energy landscape over two torsion angles/dihedrals (C1-S2-N-S1 and S2-N-S1-C2) of isolated $TFSI^-$. The stable/metastable state A–D are separated by transition states (TSs). The white dashed lines for boundaries roughly separating the *cis* and *trans* conformer regions. (b) Newman projection of the structural snapshots corresponding to the characteristic points indicated in panel (a). Two distinct *trans–trans*

isomerization pathways (I: B–C–D, & II: B–A–D) and four subpathways (1–4) for *cis*–*trans* isomerization with relative energies. (c) Scheme of two types of motion adopted by S–N–S bond angle, accompanied by a unidirectional 300° rotation of S2–C1 bond: 180° out-of-plane bond-angle rotation (BAR) inducing M(left-handed)-to-P(right-handed) helix inversion (left) and oscillation on either side of the S1–C2 bond (right).

Negative hyperconjugation. Conjugation effect is known to play a critical role in stabilizing molecular struture and enlarging torsional energy barriers. The two lone pairs of electron from nitrogen, LP_A formed by deprotonation takes sp^2 hybridization, whereas LP_B is in a p orbital (Figure 2a, left up), distinct from the general sp^3 hybridization in common sulfonamides[32-34]. Natural bond orbital (NBO) anlysis shows that the π-type nitrogen lone pair (π_N) and oxygen lone-pair (π_O) NBOs overlap with σ*(S1–C2) antibond (left bottom). Their much larger interaction energies $E(2)$ (17.78 kcal mol^{-1}, 21.73 kcal mol^{-1}, and 23.70 kcal mol^{-1}), make π_N and π_O NBOs become the dominant contributors to the high NBO occupancy (0.34e) of σ*(S1–C2) (Table S2), in comparision with π_F (~9.0 kcal mol^{-1}). The negative $\pi_{O\&N} \rightarrow$ σ*(S1–C2) hyperconjugation leads to $\pi_{O\&N} \rightarrow$ 3p(S) donation and further facilitates the formation of π_{SO} bonds and π_{SN} bond, and their conjugation among $–N^-–SO_2–$ (middle up), reflected by the highest occupied molecular orbitals (HOMOs) of the extremely staggered and eclipsed conformations (middle bottom). The shorter length of S–N bond (~1.605 Å) (Table S2 shows bond lengths and angles for selective conformations of $TFSI^-$) also implies the presence of S–N π-bonding relative to the normal value of ~1.648 Å in sulfonamides[33, 34]. Other electron donor-acceptor pairs may exist, but the σ*(S1–C2) acceptor orbital (0.14 a.u) is much more stable than others,

such as σ*(S1–N) (0.21 a.u.) and σ*(S1–O1) (0.40 a.u.) (Table S3), which renders the more favorable donation of π_O and π_N to σ*(S1–C2).

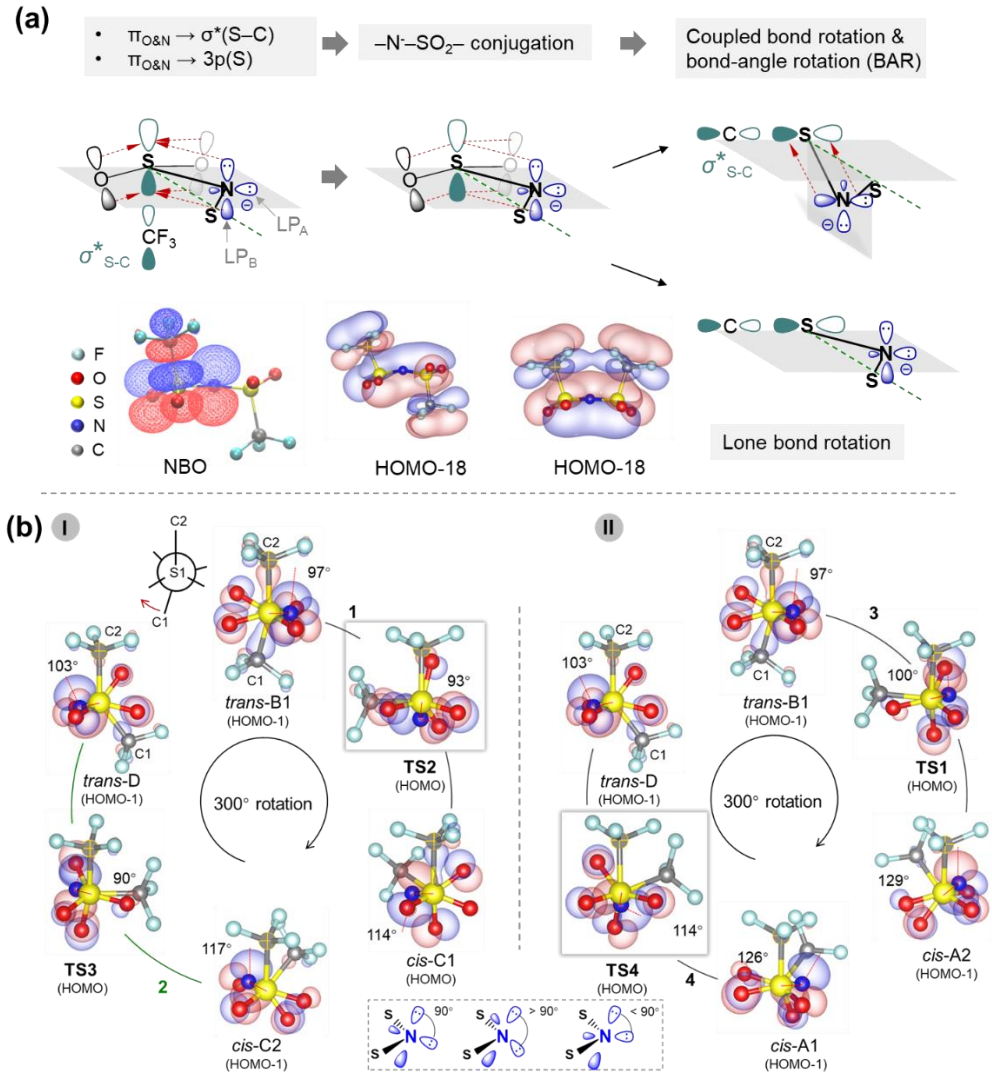

Figure 2. (a) Scheme for donation of nitrogen lone pair B (LP_B) and oxygen lone pairs which are in p orbitals, into the σ* antibonding orbitals of S–C bond (left top). Overlapped natural bond orbitals (NBOs) on the extremely staggered conformation (isosurface value of 0.05) (left bottom). Π_{SO} bonds, π_{SN} bond, and their conjugation among –N^-–SO_2– (middle top), and highest occupied molecular orbitals (HOMOs) of the extremely staggered and eclipsed conformations (middle bottom) (isosurface value of 0.009). Alternative motions around the S-S axle: coupled rotation of S–C bond with S–N–S bond angle for

maintaining conjugation (right top), and lone S–C bond rotation for interrupting conjugation (right bottom). (b) HOMOs of characteristic conformations in two isomerization pathways (I & II) with isosurface value of 0.059. Inset, distortion of trigonal planar nitrogen.

The preculiar π-conjugation enables $TFSI^-$ to carry out two possible types of internal motion around the S-S axle (Figure 2a): the unprecedented coupled bond rotation with bond-angle rotation (BAR) for maintaining conjugation (right top) and the lone bond rotation for interrupting conjugation (right bottom). The spatial evolution of molecular orbitals (MOs) (Figure 2b) elucidates that, in pathway **I**, LP_B is initially in a balanced position aligned with both S–C bonds in *trans*-B1. Subsequently, it only keeps aligned with S2–C1 bond when $TFSI^-$ converts into TS2 by the coupled S–N–S BAR with S2–C1 bond rotation. Then, it tunes its aligned objective into S1–C2 bond during the TS2-to-*cis*-C1 process, leading to the decoupling of the rotary motions. By nitrogen oscillating, it tunes its alignment with S1–C2 bond in the following *cis*-C1-to-*trans*-B1 process, and finally settles in another position in line with both S–C bonds. In pathway **II**, the order of its alignment with one of S–C bonds is reversed. In both pathways, the trigonal planar structure of nitrogen undergoes geometric deformations to different extents (Figure 2b insets & Figure S1), but the energetically favourable π-electron delocalization is preserved.

The geometric structure of a molecule is also influenced by intramolecular steric repulsions. The steric clash between two aligned S–C bonds, S–C bond with S–O bond, and two S–O bonds are well-known, but the replusion from nitrogen LP_A with S–C bonds and S–O bonds is easily overlooked (Figure S2). Furthermore, our Bader charge analysis (Table S4 & Figure S3) exhibits that each *cis*-*trans* isomerization process experiences

~0.3e intramolecular charge transfer mainly between carbon atom and fluorine atom, which suggests the dynamic repulsion between S–CF_3 moieties and S–O bonds. The net effect from the dynamic negative hyperconjugation and the five distinct steric repulsions drives $TFSI^-$ to isomerize into six diastereomeric conformers with diverse and unusually high energy barriers, rather than three pairs of enantiomers reported by previous studies.[14-18]

Countercation effect. Two typical countercations, pyrrolidinium-based PYR_{13}^+ and imidazolium-based $BMIM^+$, are chosen to examine their impact on the isomerization of $TFSI^-$ in the bulky ionic liquid state by performing AIMD simulations. Figure 3a–3f show the combined probability distribution of characteristic dihedrals of $TFSI^-$ evolving with time in the bulk PYR_{13}TFSI and BMIMTFSI. The conformational distribution of $TFSI^-$ indicates that, no *trans*-to-*cis* isomerization occurs in bulk PYR_{13}TFSI during 30 ps (Figure 3a–3c). In fact, some transition states between *cis*-C and *trans*-B even turn back to *trans* conformer. By contrast, in bulk BMIMTFSI (Figure 3d–3f), some $TFSI^-$ anions initially adopt *trans* isomer or transition states in B region, but after 30 ps, they completely convert into *cis*-C. These observations point out the preferential stabilization of *cis*-$TFSI^-$ in bulk BMIMTFSI than PYR_{13}TFSI, which conflicts the widely accepted *cis*: *trans* ratio of 1:1. In order to further quantify the conformational propensity of $TFSI^-$ in the two bulk ILs, we compare their Raman spectra computed from AIMD simulation (Figure S4 & S5), which are not accessible by static calculations. The conformer population distribution (Figure 3g) derived from the simulated Raman spectra exhibits that 60% of $TFSI^-$ adopt *trans* conformer in bulk PYR_{13}TFSI, whereas *cis*-$TFSI^-$ occupies 60% of population in bulk BMIMTFSI. This prediction is confirmed by the experimental Raman spectra analysis

(Figure 3h & Figure S6). Specifically, *cis*-$TFSI^-$ (67.11%) prevails in the bulk BMIMTFSI whereas it's less populated (41.96%) in bulk $PYR_{13}TFSI$, which are derived by deconvoluting characteristic peaks centered at 397 and 405 cm^{-1} for *trans*-$TFSI^-$ and *cis*-$TFSI^-$ (Figure 3i-3k).[35-37]

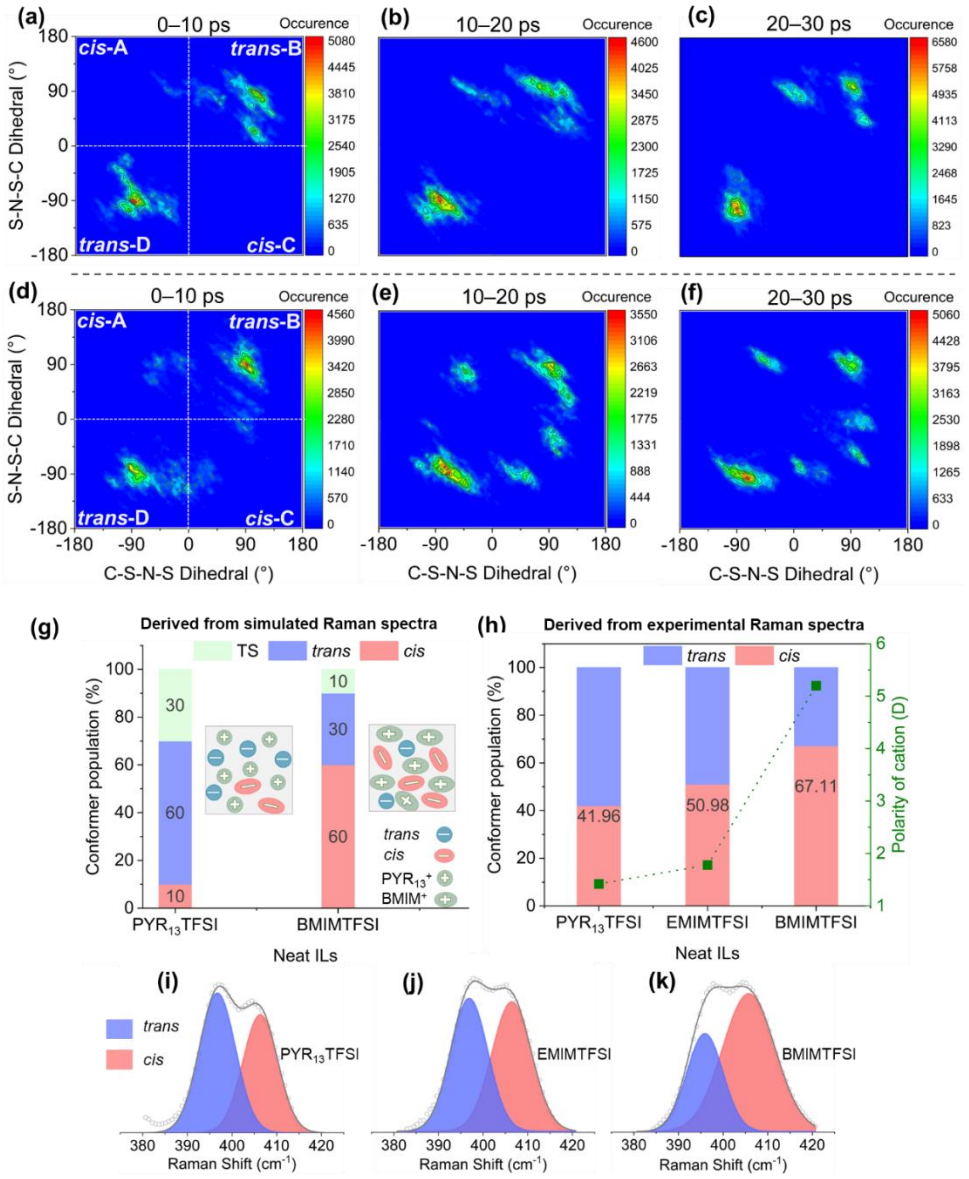

Figure 3. Combined dihedrals (C1-S1-N-S2 and S1-N-S2-C2) distribution of $TFSI^-$ evoluting over time (a) 0–10 ps, (b) 10–20 ps, (c) 20–30 ps in bulk $PYR_{13}TFSI$ and (d) 0–10 ps, (e) 10–20 ps, (f) 20–30 ps in bulk BMIMTFSI. Fractional population distribution of $TFSI^-$ conformers over cations with various polarities in the bulk ILs, derived from (g) simulated Raman spectra and (f) experimental Raman spectra. (Insets) Scheme for *trans*/*cis*-$TFSI^-$ population distribution in bulk ILs.

To probe the nature of the countercation-dependent conformational preference of $TFSI^-$, we analyzed the differences in structures and physicochemical properties between *cis*-$TFSI^-$ and *trans*-$TFSI^-$, PYR_{13}^+ and $BMIM^+$, respectively. *cis*-$TFSI^-$ and *trans*-$TFSI^-$ have almost identical polarizability (Table S5), but *cis*-$TFSI^-$ has signficantly larger dipole moment (4.44 D for *cis*-C1) than *trans*-$TFSI^-$ (1.61 D for *trans*-D) (Table 1). The AIMD sampling trajectories show that both PYR_{13}^+ and $BMIM^+$ also adopt two main conformers in the bulky systems, which is induced by flexible side alkyl chains. *cis*-PYR_{13}^+ (1.12 D) with a N-C-C-C dihedral of 65° is slightly less polar than *trans*-PYR_{13}^+ (dihedral of 171°, 1.42 D) (Figure S7a). The 0.32:1 ratio of *cis*-PYR_{13}^+ to *trans*-PYR_{13}^+ in the accumulated frequency of occurrence indicates that *cis*-PYR_{13}^+ is the minor conformer of PYR_{13}^+ in bulk. By contrast, *cis*-$BMIM^+$ (N-C-C-C dihedral of 60°, 4.44 D) has the probability of 61.24% whereas *trans*-$BMIM^+$ (N-C-C-C dihedral of 180°, 5.96 D) possesses the probability of 38.76% in all possible conformations of $BMIM^+$ (Figure S7b). The conformational geometry and distribution analysis of the countercations reveals that PYR_{13}^+ is intrinsically weakly polar, independent of its isomers, whereas $BMIM^+$ is strongly polar. Therefore, we infer that the polarity of counteraction contributes to the stereoselective isomerization of $TFSI^-$ in $TFSI^-$-based bulk ILs. The relationship is also

found in bulk EMIMTFSI (Figure 3h & 3g), where $EMIM^+$ cation (1.13–1.78 D) has a shorter alkyl chain than $BMIM^+$ (Figure S7d). To further support the inference, we also investigated the conformational distributions of $BMIM^+$ and $TFSI^-$ in bulk BMIMTFSI initiating with *cis*-$TFSI^-$, compensating the narrow scope of sampling by AIMD simulation in the limited time. The majority of *trans*-$BMIM^+$ (62.83%, 5.96 D) corresponds to the dominant population distribution of *cis*-$TFSI^-$ in the latter bulk (Figure S8), whereas the minority of *trans*-$BMIM^+$ (38.76%) matches the less population of *cis*-$TFSI^-$ in the first bulk BMIMTFSI (Figure 3d–3f). This comparison uncovers the $TFSI^-$-countercation mutual conformational selectivity and their coupled isomerization behavior. Altogether, we propose that the proportion of *cis*-$TFSI^-$ in $TFSI^-$-based bulk ILs is positively correlated with the polarity of countercations.

Table 1. Dipole moments for cationic/anionic components of ILs, and solvents in this work.

	Dihedral	Dipole moment (D)		
Isolated $TFSI^-$	5.06 (eclipsed)	4.44 (*cis*-C1)	1.61 (*trans*-D)	0.84 (staggered)
Interfacial $TFSI^-$	C-S-S-C	5.70 (*cis*,15°)	5.03 (*cis*, 77°)	1.95 (*trans*, 153°)
$EMIM^+$	C-N-C-C	1.13 (8.6°)	1.78 (124°)	1.76 (159°)
$BMIM^+$	N-C-C-C	-	4.44 (*cis*, 60°)	5.96 (*trans*, 176°)
PYR_{13}^+	N-C-C-C	-	1.12 (*cis*, 65°)	1.42 (*trans*, 171°)
PYR_{14}^+	N-C-C-C	-	2.87 (*cis*, 65°)	3.27 (*trans*, 180°)
		Gas phase	Liquid phase	
NMP	-	4.03	4.06 (CFF)[38]	4.09 (Exp.)[39]
DMSO	-	3.99	4.96 (CFF)[40]	4.06 (Exp.)[41]

CFF: Classical Force Field. Exp.: Experimental data. Interfacial $TFSI^-$: BMIMTFSI-water interface starting with *cis*-$TFSI^-$

To explore the intrinsic origin of the polarity-dependent conformational selectivity, the torsional free energy landscapes were sampled for $TFSI^-$ in gaseous cation-anion pairs. For $PYR_{13}TFSI$ (Figure 4a), *trans*-$TFSI^-$ is the most stable conformer with the global minimum energy of -142 kJ mol^{-1} in the D region, much lower than the local minimum of -116 kJ mol^{-1} (A1) for *cis*-$TFSI^-$. Other local minima corresponding to *trans*-$TFSI^-$ are also deeper than the local minima for *cis*-$TFSI^-$ (Table S6). Futhermore, the lowest $\Delta G^{\ddagger}_{\text{trans-cis}}$ increases to 54 kJ mol^{-1} (B3–TS2–C1) from 20 kJ mol^{-1} for isolated $TFSI^-$ (D–TS3–C in Figure 1a), whereas the lowest $\Delta G^{\ddagger}_{\text{cis-trans}}$ holds the same value (12 kJ mol^{-1}, C2–TS3–D). Thus, PYR_{13}^+ not only favors *trans*-$TFSI^-$ thermodynamically, but also hinders the *trans*-to-*cis* conversion of $TFSI^-$ kinetically. For BMIMTFSI (Figure 4d), *cis*-C (-84 kJ mol^{-1}) demonstrates the global minimum in the free energy profile whereas *trans*-$TFSI^-$ is slightly less stable at the local minima of B (-80 kJ mol^{-1}) and D (-76 kJ mol^{-1}), which implies that $BMIM^+$ supports *cis*-$TFSI^-$ thermodynamically. Moreover, the lowest $\Delta G^{\ddagger}_{\text{trans-cis}}$ keeps the same value (20 kJ mol^{-1}, D–TS4–A) with that of isolated $TFSI^-$, whereas the lowest $\Delta G^{\ddagger}_{\text{cis-trans}}$ increases to 24 kJ mol^{-1} (A–TS4–D). That is, $BMIM^+$ exerts completely opposite control on the $TFSI^-$ isomerization in both thermodynamics and kinetics in comparision with PYR_{13}^+. The conformational energy surfaces of $TFSI^-$ are also daramatically modulated by another two moderately polar cations, $EMIM^+$ and PYR_{14}^+ (2.87–3.27 D) (Details in Table S6 and Figure S7). To more clearly quantify the impact of countercations with various polarities on the stabilization of $TFSI^-$ conformers, we extract all energy minima from the complex landscapes and calculate the ratio of *cis*-$TFSI^-$ to *trans*-$TFSI^-$ in overall energies ($r = E_{cis}/E_{trans}$). Figure 4e displays that the ratios are in a linear relationship with the polarities of cations from the four ion pairs. This result is excellently consistent

with the correlation between fractional population of *cis*-TFSI$^-$ and polarities of cations, which is found in the bulky systems (Figure 3h).

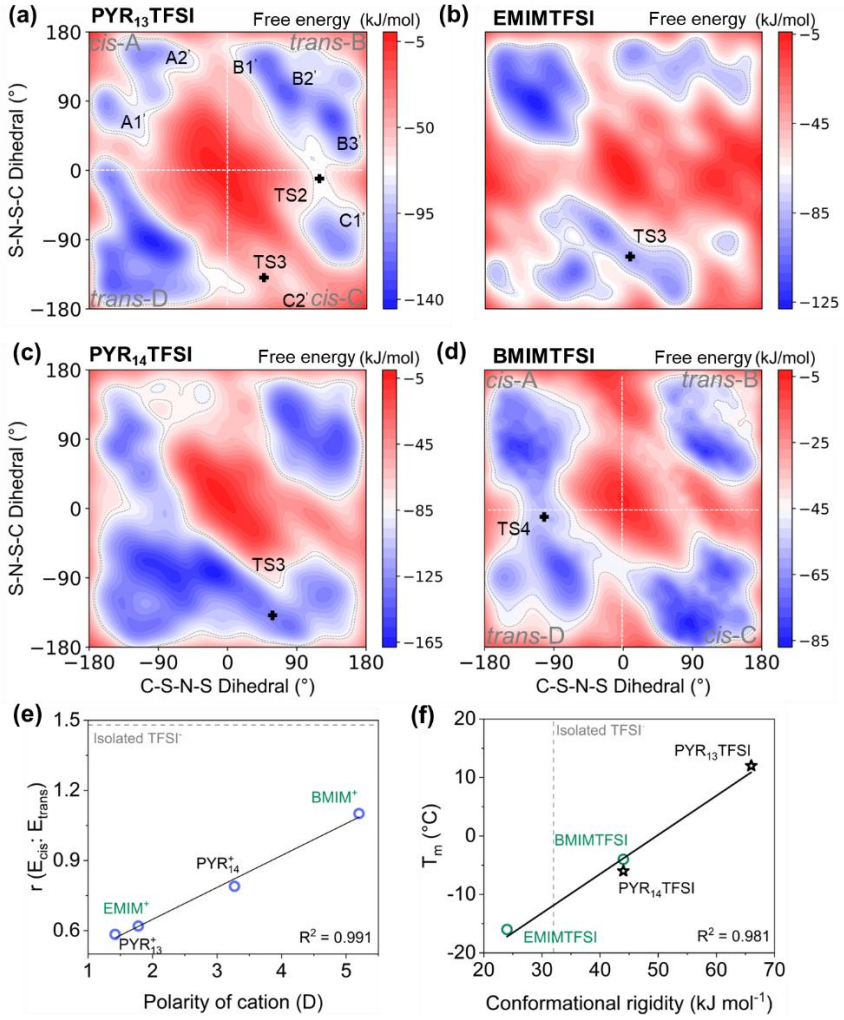

Figure 4. Torsional free-energy landscapes of TFSI$^-$ in gaseous ion pair of (a) $PYR_{13}TFSI$, (b) EMIMTFSI, (c) $PYR_{14}TFSI$, and (d) BMIMTFSI. (e) Ratio of *cis*-TFSI$^-$ to *trans*-TFSI$^-$ in overall energies ($r = E_{cis}/E_{trans}$) as a function of the polarity of countercations. The overall free energy is a sum of all energy minima. (f) Correlation of ILs melting point (T_m) with the conformational rigidity of TFSI$^-$ in ion pairs.

Conformational rigidity of $TFSI^-$. cis alkenes, the molecular systems, tend to have lower melting points (T_m) than trans alkenes due to their higher polarity and lower symmetry.[42, 43] Although we have confirmed that the proportion of *cis*-$TFSI^-$ increases with the polarity of countercations, the melting points don't drop down as the general trend. In fact, $PYR_{14}TFSI$/EMIMTFSI is the minimum turning point of the curve displaying melting points of pyrrolidinium-based (green line) or imidazolium-based (blue line) ILs over the alkyl-chain length of contercation (Figure S9). By quantatively comparing ILs with alkali halides, a latest study[44] proposes that the charateristic low T_m of ILs, relative to other salts, mainly origin from the structural entropy (configurational and conformational entropy), particularly configurational/interionic entropy, rather than the widely believed enthalpy (coulombic interaction and lattice energy). However, only conformational entropy from the cations ($EMIM^+$ & $BMIM^+$) is considered in that study, since anion PF_6^- is rigid and not deformed. By contrast, $TFSI^-$-based ILs are much more complex in additional conformational diversity of $TFSI^-$, interionic conformational selectivity and coupled isomerization, and configurational diversity. Accordingly, it's challenging to decompose enthalpy/entropy into individual terms, and consequently identify their role in the low T_m of ILs. Here, we find that the conformational rigidity (a sum of the lowest $\Delta G^{\ddagger}_{trans\text{-}cis}$ and $\Delta G^{\ddagger}_{cis\text{-}trans}$) of $TFSI^-$ in the ion pair state, is a fundamental descriptor to quantify the impact of countercations on the melting points of $TFSI^-$-based ILs (Figure 4f). The free-energy-based dynamic descriptor comprehensively including the enthalpic and entropic contribution from intraionic and interionic interactions, delineates the disorder potential of $TFSI^-$-based ILs under thermal stimuli.

Solvent effect. Although the applications of the electrolytes comprising $TFSI^-$-based ILs[45] or $M^{n+}(TFSI^-)_n$ (M = Li, Mg, Al …) salts[46-48] with solvents are ubiquitous in electrochemical energy storage systems, there are no reports on quantifying the conformational proportion of $TFSI^-$ in the solutions, which potentially influences the thermal/electrochemical properites of electrolytes, such as stability, interfacial capacitance and ionic conductivity.[49-51] We collected the Raman spectra of the solutions comprising $TFSI^-$-based ILs with polar, aprotic solvents, and quantified the impact of solvents on the population distribution of *cis/trans* conformers of $TFSI^-$ at various concentrations. Figure 5a shows that the ratio of *cis*-$TFSI^-$ in the three solutions containing $PYR_{13}TFSI$, EMIMTFSI and BMIMTFSI are all raised by 1-Methyl-2-pyrrolidone (NMP) (4.09 D and Figure S10a for the Raman spectrum of neat NMP), evidenced by the higher peak intensity at 405 cm^{-1} relative to 397 cm^{-1} (left three), and the enlarged fractional population of *cis*-$TFSI^-$ corresponding to the decreased concentration of ILs (right one). Even though for $PYR_{13}TFSI$ with weakly polar cation and high $\Delta G^{\ddagger}_{trans\text{-}cis}$ ($\geq$ 54 kJ mol^{-1}), the increased fractional population of *cis*-$TFSI^-$ reaches 27% at the concentration of 1: 5 (molar ratio). Another solvent, namely dimethyl sulfoxide (DMSO) (4.06 D and Figure S10b for the Raman spectrum of neat DMSO) exhibits its better promotion performance in the larger raise of *cis*-$TFSI^-$ fractional population (35%) in $PYR_{13}TFSI$-DMSO solution (molar ratio of 1: 5) relative to neat $PYR_{13}TFSI$, making *cis*-$TFSI^-$ fully dominate in the solution (Figure 5b). We also examined the torsional free energy surface of $TFSI^-$ in the ion pair of $PYR_{13}TFSI$ dissolved in bulk DMSO. Figure 5c–5d indicate *cis*-$TFSI^-$ is more stable in the solution with two lower local energy minima of -134 kJ mol^{-1} (A2' & C'), in contrast to -116 kJ mol^{-1} (A1) and -108 kJ mol^{-1} (C1) in the ion pair of $PYR_{13}TFSI$. As a result, the

minimum $\Delta G_{trans\text{-}cis}$ drops to 8 kJ mol^{-1}, versus 26 kJ mol^{-1} in the neat $PYR_{13}TFSI$. Moreover, the *trans*-to-*cis* isomerization is catalyzed by DMSO through the energy pathway of B1'–TS1'–A2' (minimum $\Delta G^{\ddagger}_{trans\text{-}cis}$ = 12 kJ mol^{-1}), saving 78% of the energy and even lower than that in isolated $TFSI^-$ ($\geq$ 20 kJ mol^{-1}). The $\Delta G^{\ddagger}_{trans\text{-}cis}$ in other pathways also drop to different degrees. On the other hand, the minimum $\Delta G^{\ddagger}_{cis\text{-}trans}$ jumps from 12 kJ mol^{-1} (C2–D, gaseous $PYR_{13}TFSI$) to 42 kJ mol^{-1} (A1'–TS4'–D2'). The energy analysis reveals that strongly polar solvents stabilize *cis*-$TFSI^-$, catalyze the *trans*-to-*cis* process, and hinder the reverse transition, which breaks most of the constraints exerted on $TFSI^-$ by PYR_{13}^+.

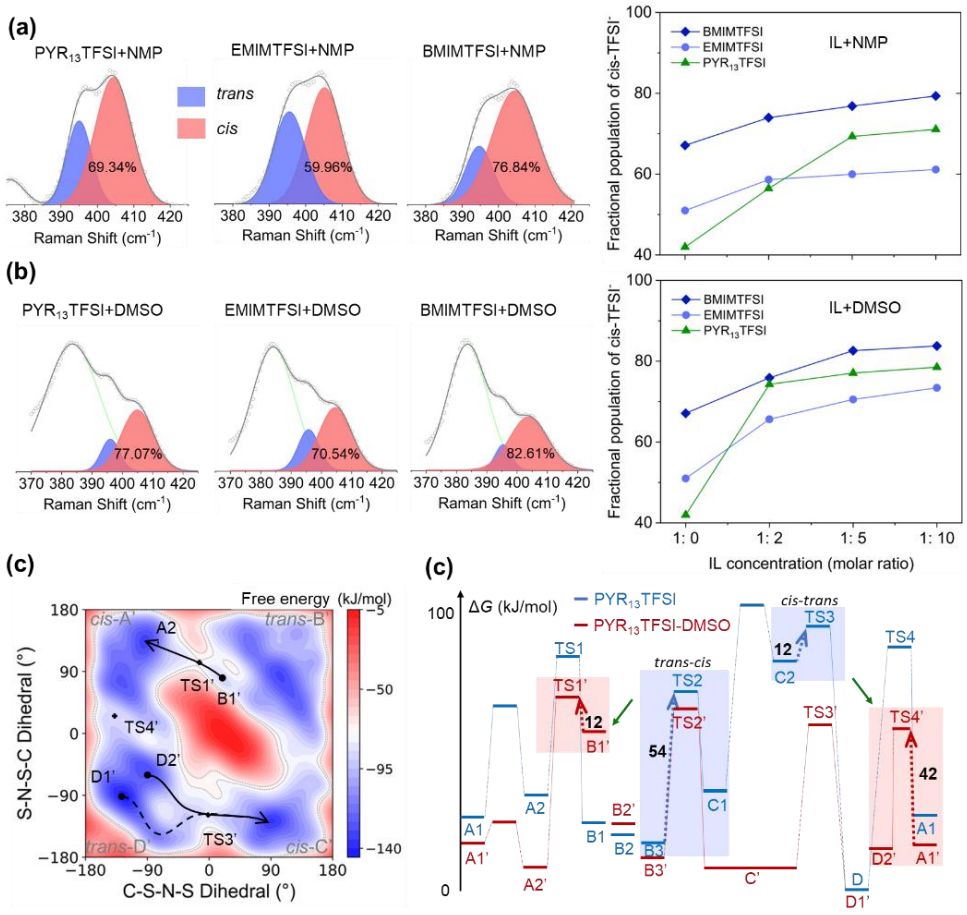

Figure 5. (a & b) Characteristic Raman spectra of IL-solvent solutions at molar ratio of 1: 5 and IL concentration-dependent fractional population of *cis*-$TFSI^-$, derived from peak deconvolution. The ILs include $PYR_{13}TFSI$, EMIMTFSI and BMIMTFSI. NMP, 1-Methyl-2-pyrrolidone. DMSO, dimethyl sulfoxide. (c) Torsional free-energy landscape of $TFSI^-$ in ion pair of $PYR_{13}TFSI$ dissolved in bulk DMSO (explicit solvent model) and its comparison with $TFSI^-$ isomerization in neat ion pair of $PYR_{13}TFSI$ (d). Red and blue regions display the minimum energy pathways.

Local environment effect. Based on the understanding of the strong $TFSI^-$-cation (two-body) interaction, we have extended our exploration to the $TFSI^-$-cation-solvent (many-body) system. Although the dipolar interactions are inherently anisotropic[52] in the IL-solvent solutions, the environment of the ion pair is homogeneous, since each solvent molecule is identical in shape and polarity. Nevertheless, bulk $TFSI^-$-based ILs consisting of two strongly interacting components with deformable structures and diverse polarities, exhibit additional anisotropy and heterogeneity, which further complicates the analysis of $TFSI^-$ isomerization in the ion pair dissolved in the "$TFSI^-$-based IL solution". The trajectories of two bulky BMIMTFSI systems initiating with *trans*-$TFSI^-$/*cis*-$TFSI^-$, show that both stay as *trans* conformer during 30 ps (Figure S11a–11c & Figure S12a–12c), but *trans*-TFSI#1 is surrounded by one *cis*-$TFSI^-$, one TS and four *trans*-$TFSI^-$ (Figure 6a, left), whereas *trans*-TFSI#1* is environed by five *cis*-$TFSI^-$ and one TS (Figure 6b, left). By metadynamics approach again, we can obtain the whole conformational space of *trans*-TFSI#1 and *trans*-TFSI#1* while maintaining their coupling with environments and characterize the impact of surrounding ions on their isomerization. The conformational free-energy surface of *trans*-TFSI#1 (*trans*-B) seems to resemble the landscape of gaseous

BMIMTFSI ion pair (Figure 4d), but the energy difference between *cis*-C and *trans*-B increases from 4 kJ mol^{-1} to 12 kJ mol^{-1} while the lowest $\Delta G^{\ddagger}_{\text{trans-cis}}$ or $\Delta G^{\ddagger}_{\text{cis-trans}}$ jumps by 20 kJ mol^{-1} (Figure 6a, right). In a sharp contrast, *trans*-TFSI#1* (*trans*-D) overmatches its competing *cis* conformers with the environment in a large energy difference of 28–42 kJ mol^{-1} and high $\Delta G^{\ddagger}_{\text{trans-cis}}$ of 46–70 kJ mol^{-1} (Figure 6b, right). These simulation results signigy that the local environment in the bulky TFSI^{-}-based IL systems also influence the conformational stability and rigidity of TFSI^{-} by net electrostatic interactions, in addition to the countercations, suggesting the complex many-body correlation[52, 53].

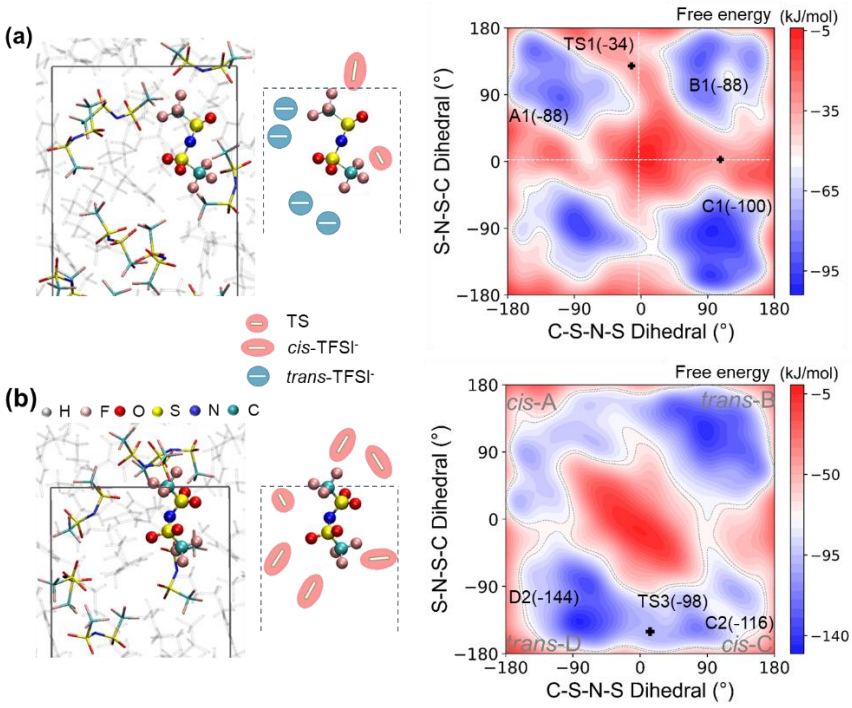

Figure 6. Snapshots (left) at 30-ps AIMD trajectories and torsional free-energy landscapes (left) of TFSI#1 (a) in the bulk BMIMTFSI initiating with *trans*-TFSI^{-}, and TFSI#1* (b) in the bulk BMIMTFSI initiating with *cis*-TFSI^{-}. Black solid line and blue dashed line (scheme) illustrating the unit cell. Cations are displayed in grey stick model.

Conclusions

The conventional static electronic structure calculation of isolated $TFSI^-$ showed that the sole and extremely low energy barrier between *cis* and *trans* conformer endowed the conformational flexibility of $TFSI^-$, which might contribute to the unusual thermal and mechanical properties of ILs. By using AIMD combined with metadynamics, we revealed that gaseous $TFSI^-$ experiences restricted *cis-trans* isomerization following four distinct pathways with strikingly higher and diverse free-energy barriers. We have identified an unprecedented coupled motion comprising bond rotation and bond-angle rotation at the central N^-, which competes with other two isomerization mechanisms in $TFSI^-$, a system with bicoordinated heteroatoms. Discovering theoretical evidence for the 180° bond-angle rotation also brings our knowledge one step further towards an alternative strategy for controlling the molecular helical inversion, dynamic chirality and unidirectional rotation of molecular motor. The negative $\pi_{O\&N} \rightarrow \sigma^*(S–C)$ hyperconjugation leads π electrons to delocalize among $–SO_2–N^-–SO_2–$ and allows $TFSI^-$ to carry out the coupled motion for maintaining conjugation. The net dynamic effect from the negative hyperconjugation and five distinct steric repulsions drives $TFSI^-$ to rigidly and diversely isomerize into six diastereomeric conformers, rather than three pairs of enantiomers.

Countercations can significantly control the conformational stability and rigidity of $TFSI^-$. The overall stability of *cis*-$TFSI^-$ linearly increases with the polarity of countercations in the isolated ion pair state. The fractional population of *cis*-$TFSI^-$ follows the same trend in bulk ILs, which is confirmed by both experiments and simulations. The

conformational rigidity of $TFSI^-$ in the ion pair, a free-energy-based dynamic descriptor, can excellently quantify the impact of countercations on the T_m of $TFSI^-$-based ILs, owing to the inclusion of cation-anion coupling. This relationship provides new fundamental insights into the origin of low T_m of ILs. The unified descriptor can serve as a guideline towards the rational design of low-T_m ILs. The similar effects including *cis*-$TFSI^-$ stabilization, *trans*-to-*cis* catalysis, and reverse transition hinderance are also found in strongly polar solvents which overcomes most of the constraints imposed on $TFSI^-$ by countercations. The distinct local environments in the highly anisotropic and heterogeneous $TFSI^-$-based IL bulks can exert different additional influence on the isomerization behavior of $TFSI^-$ by net electrostatic interactions. This feature in association with interionic mutual conformational selectivity and coupled isomerization imply that $TFSI^-$-based ILs are the complex many-body strongly correlated systems.

The counterintuitive isomerization behavior of $TFSI^-$ and its correlation with distinct environments can also provide molecular level basis for multiple other exotic thermal/mechanical/electrical properities of ILs. (1) The diversity in the relative stabililty of conformers, isomerization pathway and energy barrier of $TFSI^-$ leads to the peculiar sequence of phase transitions over temperature, phase-dependent transport characteristics and interfacial capacitance. (2) Pressure forces *trans*-*cis* conversion (helical folding) of $TFSI^-$, cation-anion reconfiguration, and re-orientation of those dipoles, thus induces liquid-liquid transition and direct piezoelectric effect, a first report in a neat liquid. (3) The alignment of ion dipoles also forms long-lived electric fields of IL bilayers under external electric field pulse.

ASSOCIATED CONTENT

Supporting Information

The Supplemental Information (including Raman spectroscopy characterization, computational details, Tables S1–S6, and Figures S1-S12) is available free of charge at https://pubs.acs.org/doi/

AUTHOR INFORMATION

Corresponding Authors

TieJun Zhang - *Department of Mechanical Engineering, Masdar Institute, Khalifa University of Science and Technology, P.O. Box 127788, Abu Dhabi, UAE;* Email: tiejun.zhang@ku.ac.ae

Author Contributions

L.Y.: conceptualization, simulation and experimental characterization; **A.R.:** experiments design and writing editing; **D.K.:** supervision, writing editing; **H.B.:** supervision; **T.Z.**: conceptualization, supervision, writing editing, funding acquisition, resources.

Notes

The authors declare no competing financial interests.

ACKNOWLEDGMENTS

This work was supported by Alibaba Cloud and the Abu Dhabi Award for Research Excellence 2019 (#AARE19-185) of ASPIRE under the Advanced Technology Research Council in Abu Dhabi, UAE. Qi Zhang Gaussian

References

1. Horner, L.; Winkler, H.; Rapp, A.; Mentrup, A.; Hoffmann, H.; Beck, P., Phosphororganische verbindungen optisch aktive tertiäre phosphine aus optisch aktiven quartären phosphoniumsalzen. *Tetrahedron Letters* **1961,** *2* (5), 161-166.

2. Brois, S. J., Aziridines. XII. Isolation of a stable nitrogen pyramid. *Journal of the American Chemical Society* **1968,** *90* (2), 508-509.

3. Smith, O.; Popescu, M. V.; Hindson, M. J.; Paton, R. S.; Burton, J. W.; Smith, M. D., Control of stereogenic oxygen in a helically chiral oxonium ion. *Nature* **2023,** *615* (7952), 430-435.

4. Rauk, A.; Allen, L. C.; Mislow, K., Pyramidal inversion. *Angewandte Chemie International Edition in English* **1970,** *9* (6), 400-414.

5. Baechler, R. D.; Mislow, K., Effect of structure on the rate of pyramidal inversion of acyclic phosphines. *Journal of the American Chemical Society* **1970,** *92* (10), 3090-3093.

6. Canfield, P. J.; Blake, I. M.; Cai, Z.-L.; Luck, I. J.; Krausz, E.; Kobayashi, R.; Reimers, J. R.; Crossley, M. J., A new fundamental type of conformational isomerism. *Nature chemistry* **2018,** *10* (6), 615-624.

7. Lehn, J. In *Nitrogen inversion: experiment and theory*, Dynamic Stereochemistry, Springer: 1970; pp 311-377.

8. Wu, Z.; Feng, R.; Xu, J.; Lu, Y.; Lu, B.; Yang, T.; Frenking, G.; Trabelsi, T.; Francisco, J. S.; Zeng, X., Photoinduced Sulfur–Nitrogen Bond Rotation and Thermal Nitrogen Inversion in Heterocumulene OSNSO. *Journal of the American Chemical Society* **2018,** *140* (4), 1231-1234.

9. Bonacic-Koutecky, V.; Persico, M., CI study of geometrical relaxation in the ground and excited singlet and triplet states of unprotonated Schiff bases: allylidenimine and formaldimine. *Journal of the American Chemical Society* **1983,** *105* (11), 3388-3395.

10. Lehn, J. M., Conjecture: imines as unidirectional photodriven molecular motors—motional and constitutional dynamic devices. *Chemistry–A European Journal* **2006,** *12* (23), 5910-5915.

11. Bharatam, P.; Kaur, D.; Senthil Kumar, P., Potential energy surface of thionylimide. *International journal of quantum chemistry* **2006,** *106* (5), 1237-1249.

12. Deng, W.-F.; Li, Y.-X.; Zhao, Y.-X.; Hu, J.-S.; Yao, Z.-S.; Tao, J., Inversion of Molecular Chirality Associated with Ferroelectric Switching in a High-Temperature Two-Dimensional Perovskite Ferroelectric. *Journal of the American Chemical Society* **2023,** *145* (9), 5545-5552.

13. Zhang, Q.; Toyoda, R.; Pfeifer, L.; Feringa, B. L., Architecture-Controllable Single-Crystal Helical Self-assembly of Small-Molecule Disulfides with Dynamic Chirality. *Journal of the American Chemical Society* **2023**.

14. Fujii, K.; Fujimori, T.; Takamuku, T.; Kanzaki, R.; Umebayashi, Y.; Ishiguro, S.-i., Conformational Equilibrium of Bis(trifluoromethanesulfonyl) Imide Anion of a Room-Temperature Ionic Liquid: Raman Spectroscopic Study and DFT Calculations. *The Journal of Physical Chemistry B* **2006,** *110* (16), 8179-8183.

15. Philippi, F.; Pugh, D.; Rauber, D.; Welton, T.; Hunt, P. A., Conformational design concepts for anions in ionic liquids. *Chemical Science* **2020,** *11* (25), 6405-6422.

16. Lassègues, J. C.; Grondin, J.; Holomb, R.; Johansson, P., Raman and ab initio study of the conformational isomerism in the 1-ethyl-3-methyl-imidazolium bis(trifluoromethanesulfonyl)imide ionic liquid. *Journal of Raman Spectroscopy* **2007,** *38* (5), 551-558.

17. Fujii, K.; Seki, S.; Fukuda, S.; Kanzaki, R.; Takamuku, T.; Umebayashi, Y.; Ishiguro, S.-i., Anion conformation of low-viscosity room-temperature ionic liquid 1-ethyl-3-methylimidazolium bis (fluorosulfonyl) imide. *The Journal of Physical Chemistry B* **2007,** *111* (44), 12829-12833.

18. Canongia Lopes, J. N.; Shimizu, K.; Pádua, A. A. H.; Umebayashi, Y.; Fukuda, S.; Fujii, K.; Ishiguro, S.-i., A Tale of Two Ions: The Conformational Landscapes of Bis(trifluoromethanesulfonyl)amide and N,N-Dialkylpyrrolidinium. *The Journal of Physical Chemistry B* **2008,** *112* (5), 1465-1472.

19. Clayden, J.; Greeves, N.; Warren, S., *Organic chemistry*. Oxford university press: 2012.

20. Liu, L.; Fang, W.-H.; Martinez, T. J., A Nitrogen Out-of-Plane (NOOP) Mechanism for Imine-Based Light-Driven Molecular Motors. *Journal of the American Chemical Society* **2023**.

21. Feng, Z.; Tantillo, D. J., Dynamic Effects on Migratory Aptitudes in Carbocation Reactions. *J Am Chem Soc* **2021,** *143* (2), 1088-1097.

22. Yang, B.; Schouten, A.; Ess, D. H., Direct Dynamics Trajectories Reveal Nonstatistical Coordination Intermediates and Demonstrate that sigma and pi-Coordination Are Not Required for Rhenium(I)-Mediated Ethylene C-H Activation. *J Am Chem Soc* **2021,** *143* (22), 8367-8374.

23. MacFarlane, D. R.; Kar, M.; Pringle, J. M., *Fundamentals of ionic liquids: from chemistry to applications*. John Wiley & Sons: 2017.

24. Capitani, F.; Trequattrini, F.; Palumbo, O.; Paolone, A.; Postorino, P., Phase transitions of PYR14-TFSI as a function of pressure and temperature: the competition between smaller volume and lower energy conformer. *The Journal of Physical Chemistry B* **2016,** *120* (11), 2921-2928.

25. Capitani, F.; Gatto, S.; Postorino, P.; Palumbo, O.; Trequattrini, F.; Deutsch, M.; Brubach, J.-B.; Roy, P.; Paolone, A., The Complex Dance of the Two Conformers of Bis (trifluoromethanesulfonyl) imide as a Function of Pressure and Temperature. *The Journal of Physical Chemistry B* **2016,** *120* (7), 1312-1318.

26. Wojnarowska, Z.; Cheng, S.; Yao, B.; Swadzba-Kwasny, M.; McLaughlin, S.; McGrogan, A.; Delavoux, Y.; Paluch, M., Pressure-induced liquid-liquid transition in a family of ionic materials. *Nature Communications* **2022,** *13* (1), 1342.

27. Bussi, G.; Laio, A.; Tiwary, P., Metadynamics: A Unified Framework for Accelerating Rare Events and Sampling Thermodynamics and Kinetics. In *Handbook of Materials Modeling*, 2020; pp 565-595.

28. Bussi, G.; Laio, A., Using metadynamics to explore complex free-energy landscapes. *Nature Reviews Physics* **2020,** *2* (4), 200-212.

29. Cheng, C.-Y.; Pai, W.-L.; Chen, Y.-H.; Paylaga, N. T.; Wu, P.-Y.; Chen, C.-W.; Liang, C.-T.; Chou, F.-C.; Sankar, R.; Fuhrer, M. S., Phase Modulation of Self-Gating in Ionic Liquid-Functionalized InSe Field-Effect Transistors. *Nano Letters* **2022**.

30. Hossain, M. I.; Blanchard, G., Ionic Liquids Exhibit the Piezoelectric Effect. *The Journal of Physical Chemistry Letters* **2023,** *14*, 2731-2735.

31. Belotti, M.; Lyu, X.; Xu, L.; Halat, P.; Darwish, N.; Silvester, D. S.; Goh, C.; Izgorodina, E. I.; Coote, M. L.; Ciampi, S., Experimental evidence of long-lived electric fields of ionic liquid bilayers. *Journal of the American Chemical Society* **2021,** *143* (42), 17431-17440.

32. Modarresi-Alam, A. R.; Amirazizi, H. A.; Bagheri, H.; Bijanzadeh, H.-R.; Kleinpeter, E., Dynamic 1H NMR Spectroscopic Study of the Ring Inversion in N-Sulfonyl Morpholines Studies on N− S Interactions. *The Journal of organic chemistry* **2009,** *74* (13), 4740-4746.

33. Zeng, X.; Gerken, M.; Beckers, H.; Willner, H., Anomeric effects in sulfonyl compounds: an experimental and computational study of fluorosulfonyl azide, FSO2N3, and trifluoromethylsulfonyl azide, CF3SO2N3. *The Journal of Physical Chemistry A* **2010,** *114* (28), 7624-7630.

34. Blahun, O. P.; Rozhenko, A. B.; Rusanov, E.; Zhersh, S.; Tolmachev, A. A.; Volochnyuk, D. M.; Grygorenko, O. O., Twisting and Turning the Sulfonamide Bond: A Synthetic, Quantum Chemical, and Crystallographic Study. *The Journal of Organic Chemistry* **2020,** *85* (8), 5288-5299.

35. Umebayashi, Y.; Mitsugi, T.; Fujii, K.; Seki, S.; Chiba, K.; Yamamoto, H.; Canongia Lopes, J. N.; Pádua, A. A. H.; Takeuchi, M.; Kanzaki, R.; Ishiguro, S.-i., Raman Spectroscopic Study, DFT Calculations and MD Simulations on the Conformational Isomerism of N-Alkyl-N-methylpyrrolidinium Bis-(trifluoromethanesulfonyl) Amide Ionic Liquids. *The Journal of Physical Chemistry B* **2009,** *113* (13), 4338-4346.

36. Kinsey, T.; Glynn, K.; Cosby, T.; Iacob, C.; Sangoro, J., Ion Dynamics of Monomeric Ionic Liquids Polymerized In Situ within Silica Nanopores. *ACS Appl Mater Interfaces* **2020,** *12* (39), 44325-44334.

37. Moschovi, A. M.; Ntais, S.; Dracopoulos, V.; Nikolakis, V., Vibrational spectroscopic study of the protic ionic liquid 1-H-3-methylimidazolium bis(trifluoromethanesulfonyl)imide. *Vibrational Spectroscopy* **2012,** *63*, 350-359.

38. Oh, Y.; Choi, H. K.; Jung, H.; Jin, J.-U.; Kim, Y.-K.; You, N.-H.; Ku, B.-C.; Kim, Y.; Yu, J., Analysis of the effect of organic solvent–sheet interfacial interaction on the exfoliation of sulfur-doped reduced graphene oxide sheets in a solvent system using molecular dynamics simulations. *Physical Chemistry Chemical Physics* **2020,** *22* (36), 20665-20672.

39. Fischer, E., The electric moment of 1-methylpyrrolid-2-one. *Journal of the Chemical Society (Resumed)* **1955**, 1382-1383.

40. Zhong, J.; Carignano, M. A.; Kais, S.; Zeng, X. C.; Francisco, J. S.; Gladich, I., Tuning the Stereoselectivity and Solvation Selectivity at Interfacial and Bulk Environments by Changing Solvent Polarity: Isomerization of Glyoxal in Different Solvent Environments. *J Am Chem Soc* **2018,** *140* (16), 5535-5543.

41. Pekary, A. E., Dipole moment and far-infrared studies on the dimethyl sulfoxide-iodine complex. *The Journal of Physical Chemistry* **1974,** *78* (17), 1744-1746.

42. Hsu, T.-W.; Kempel, S. J.; Felix Thayne, A. P.; Michaudel, Q., Stereocontrolled acyclic diene metathesis polymerization. *Nature Chemistry* **2023,** *15* (1), 14-20.

43. Smith, M. B., *March's advanced organic chemistry: reactions, mechanisms, and structure*. John Wiley & Sons: 2020.

44. Endo, T.; Sunada, K.; Sumida, H.; Kimura, Y., Origin of low melting point of ionic liquids: dominant role of entropy. *Chemical Science* **2022,** *13* (25), 7560-7565.

45. Ma, X.; Yu, J.; Hu, Y.; Texter, J.; Yan, F., Ionic Liquid/Poly (Ionic Liquid)-Based Electrolytes for Lithium Batteries. *Industrial Chemistry & Materials* **2023**.

46. Suo, L.; Borodin, O.; Gao, T.; Olguin, M.; Ho, J.; Fan, X.; Luo, C.; Wang, C.; Xu, K., "Water-in-salt" electrolyte enables high-voltage aqueous lithium-ion chemistries. *Science* **2015,** *350* (6263), 938-943.

47. Qiao, L.; Oteo, U.; Martinez-Ibanez, M.; Santiago, A.; Cid, R.; Sanchez-Diez, E.; Lobato, E.; Meabe, L.; Armand, M.; Zhang, H., Stable non-corrosive sulfonimide salt for 4-V-class lithium metal batteries. *Nat Mater* **2022,** *21* (4), 455-462.

48. Li, Z.; Rao, H.; Atwi, R.; Sivakumar, B. M.; Gwalani, B.; Gray, S.; Han, K. S.; Everett, T. A.; Ajantiwalay, T. A.; Murugesan, V., Non-polar ether-based electrolyte solutions for stable high-voltage non-aqueous lithium metal batteries. *Nature Communications* **2023,** *14* (1), 868.

49. Wahyudi, W.; Guo, X.; Ladelta, V.; Tsetseris, L.; Nugraha, M. I.; Lin, Y.; Tung, V.; Hadjichristidis, N.; Li, Q.; Xu, K., Hitherto Unknown Solvent and Anion Pairs in Solvation Structures Reveal New Insights into High-Performance Lithium-Ion Batteries. *Advanced Science* **2022,** *9* (28), 2202405.

50. Huang, Z.; Wang, T.; Li, X.; Cui, H.; Liang, G.; Yang, Q.; Chen, Z.; Chen, A.; Guo, Y.; Fan, J., Small-Dipole-Molecule-Containing Electrolytes for High-Voltage Aqueous Rechargeable Batteries. *Advanced Materials* **2022,** *34* (4), 2106180.

51. Liang, P.; Sun, H.; Huang, C. L.; Zhu, G.; Tai, H. C.; Li, J.; Wang, F.; Wang, Y.; Huang, C. J.; Jiang, S. K., A Nonflammable High-Voltage 4.7 V Anode-Free Lithium Battery. *Advanced Materials* **2022**, 2207361.

52. Yao, N. Y.; Zaletel, M. P.; Stamper-Kurn, D. M.; Vishwanath, A., A quantum dipolar spin liquid. *Nature Physics* **2018,** *14* (4), 405-410.

53. Davis, E. J.; Ye, B.; Machado, F.; Meynell, S. A.; Wu, W.; Mittiga, T.; Schenken, W.; Joos, M.; Kobrin, B.; Lyu, Y.; Wang, Z.; Bluvstein, D.; Choi, S.; Zu, C.; Jayich, A. C. B.; Yao, N. Y., Probing many-body dynamics in a two-dimensional dipolar spin ensemble. *Nature Physics* **2023**.